ISSN 0915-633X

NATIONAL INSTITUTE FOR FUSION SCIENCE

A 6MeV Heavy Ion Beam Probe for the Large Helical Device

A. Fujisawa, H. Iguchi, A. Taniike, M. Sasao and Y. Hamada

(Received – Jan. 12, 1994)

NIFS-272 Feb. 1994

RESEARCH REPORT
NIFS Series

NAGOYA, JAPAN

A 6MeV Heavy Ion Beam Probe for the Large Helical Device

A. Fujisawa, H. Iguchi, A. Taniike, M. Sasao, Y. Hamada

National Institute for Fusion Science
464-01, Furo-cho, Chikusa-ku, Nagoya, Japan

Abstract

A 6MeV heavy ion beam probe (HIBP) is designed for potential measurements on the Large Helical Device (LHD). The article describes a method to control the 3-D probing beam trajectories in the helical magnetic field, an estimate of beam attenuation and energy reduction arising from the long paths in the plasma, and a cylindrical analyzer as a candidate of the energy analyzer.

Keywords: HIBP, LHD, Trajectory Control, Beam Attenuation, Energy Reduction, Cylindrical Energy Analyzer

I. Introduction

The heavy ion beam probe[1-10], which is a unique method to permit direct measurements of internal plasma potential and fluctuations of potential and density in magnetically confined plasmas, has been developed since it was successfully applied on a hollow cathode arc plasma[1]. Extension of this method to recent large devices with stronger magnetic field makes the scale of the HIBP systems huge and expensive. The 500keV HIBP in the TEXT tokamak[4] is upgraded to the 2MeV system in order to make the observation area cover the whole plasma cross section[5].

The Large Helical Device (LHD), a heliotron/torsatron device whose magnetic field is generated by superconducting coils, is under construction. The major and averaged minor radii are 3.9m, 0.6m, respectively. The central magnetic field strength will be 3T. Three dimensional characteristics and strength of the LHD magnetic field will provide the most difficult environment for the application of HIBP. A 6 MeV HIBP project for the LHD has been developed to measure the internal plasma potential which is an essential physical quantity related to the confinement property in helical devices. This article describes the preliminary design and concept of the HIBP system for the LHD and several problems to be solved in the application of HIBP on large plasma confinement devices are discussed.

II. Trajectory Control

A. Basic Concept

The performance of HIBPs is deeply connected with the magnetic field structure of the applied confinement devices. Three dimensional beam trajectories, such as a helical device, needs a special consideration to determine the geometrical configuration of the HIBP system[11-13]. The design of the

LHD HIBP is optimized for the 3T standard magnetic configuration whose axis is located at 3.75m; the axis is shifted inward from the center of the vacuum chamber by 0.15m. The beam transport system including the accelerator and the energy analyzer will be arranged so that the probing beam from the accelerator with no sweep voltage can observe the potential on the magnetic axis of the standard magnetic configuration.

The schematic view of the HIBP system is shown in Fig. 1. The primary beam enters through a bottom port and the secondary beam comes out from the side port located 18° apart from the bottom port in toroidal direction. The beam energy of singly charged gold is 5.6MeV for the 3T standard operation. The system has two additional sets of sweep plates which are located in the analyzer side. A newly designed cylindrical analyzer is a candidate as the energy analyzer instead of the traditional 30° parallel plate energy analyzer.

The tandem type accelerator whose maximum terminal voltage is 3MeV will be installed as the probing beam injector. A negative gold ion source[14] has been developed for 3T operation; then the maximum beam energy is 6MeV. For the operation of half magnetic field strength, this accelerator is also used as a 3MeV single end one by substituting the charge stripping cell with the thermal thallium or other sources.

B. Active Control of Probing Beam Trajectories

One of the troublesome problems inherent with 3-D trajectories is that the secondary beam incident angle into the aperture of the energy analyzer varies two dimensionally depending on the birth point of the secondary beam (the observation point) and magnetic field configurations. The displacement of the beam position and the change of the beam incident angle on the plane

including the aperture of the energy analyzer are expressed as

$$\Delta X_{\mathrm{D}} = \frac{\partial X_{\mathrm{D}}}{\partial K_0}\Delta K_0 + \sum \frac{\partial X_{\mathrm{D}}}{\partial E_i}\Delta E_i + \sum \frac{\partial X_{\mathrm{D}}}{\partial I_i}\Delta I_i + \frac{\partial X_{\mathrm{D}}}{\partial \rho}\Delta\rho \qquad (1)$$

$$\Delta Y_{\mathrm{D}} = \frac{\partial Y_{\mathrm{D}}}{\partial K_0}\Delta K_0 + \sum \frac{\partial Y_{\mathrm{D}}}{\partial E_i}\Delta E_i + \sum \frac{\partial Y_{\mathrm{D}}}{\partial I_i}\Delta I_i + \frac{\partial Y_{\mathrm{D}}}{\partial \rho}\Delta\rho \qquad (2)$$

$$\Delta \theta_{\mathrm{D}} = \frac{\partial \theta_{\mathrm{D}}}{\partial K_0}\Delta K_0 + \sum \frac{\partial \theta_{\mathrm{D}}}{\partial E_i}\Delta E_i + \sum \frac{\partial \theta_{\mathrm{D}}}{\partial I_i}\Delta I_i + \frac{\partial \theta_{\mathrm{D}}}{\partial \rho}\Delta\rho \qquad (3)$$

$$\Delta \phi_{\mathrm{D}} = \frac{\partial \phi_{\mathrm{D}}}{\partial K_0}\Delta K_0 + \sum \frac{\partial \phi_{\mathrm{D}}}{\partial E_i}\Delta E_i + \sum \frac{\partial \phi_{\mathrm{D}}}{\partial I_i}\Delta I_i + \frac{\partial \phi_{\mathrm{D}}}{\partial \rho}\Delta\rho \qquad (4)$$

where K_0, E_{i}, ρ mean the beam energy, the electric field between the sweep plates, a parameter indicating the ionization point, respectively, and I_{i} represents a coil current generating the LHD magnetic field, Δ means an infinitesimal change.

The left-hand-side values of ΔX_{D}, ΔY_{D}, $\Delta \theta_{\mathrm{D}}$, $\Delta \phi_{\mathrm{D}}$ arising from the changes of ΔK_0, ΔI_i, $\Delta\rho$ can be canceled out by choosing an appropriate combination of four parameters ΔE_1, ΔE_2, ΔE_3, ΔE_4. This means that the probing beam trajectory can be controlled completely if HIBP systems have four sets of sweep plates. As a result, the introduction of two additional sets of sweep plates allows to obtain two dimensional potential distribution and to adjust the beam trajectory easily to different magnetic configuration. The method is now being tested in the Compact Helical System (CHS) which is a heliotron/torsatron device[13].

C. Observation Range

By integrating Eq. (1) under the condition of $\Delta K_0 = \Delta I_i = 0$ with respect to $\Delta\rho$, we can obtain a series of the electric field strengths to make the secondary beam trajectories pass at the analyzer aperture position with a constant incident angle. In the present calculation, the parameter ρ is

chosen to be the toroidal angle of the ionization point ξ_{ion}. Figure 2 shows the electric fields as a function of the toroidal angle of the ionization position, and the corresponding observation points which are projected onto the magnetic surface at a toroidal angle $\xi = 0$ since the observation points, in fact, are distributed in the toroidal direction. Several examples of trajectories are demonstrated in Fig. 3. The primary beam directed backward initially to the side port where the secondary beam comes out, and the secondary trajectories are piled up on a line after the point represented by a circle. Suppose a polar coordinate where the vertical and the radial directions coincide with polar axis, x-axis, respectively, then the injection angle of the standard probing beam to observe the magnetic axis is $\theta = 7.8°$, $\phi = 205°$.

In order to measure the plasma potential from the center to the edge, the electric field strengths, as shown in Fig. 2, are quite large. The opening of the sweep plates should be wide enough to allow the bundle of the beam trajectories to enter. If the width of the opening is assumed to be 0.5m, the maximum sweep voltage reaches at about 100kV. Controlling such a large sweep voltage under strong UV radiation from the plasma is one of the issues to require research and development.

III. Probing Beam Interaction with Plasma

The path lengths of the primary and secondary beam trajectories are shown in Fig. 4 as a function of the toroidal angle of the ionization point ξ_{ion}. The lengths of the primary and secondary beam trajectories observing the potential at the magnetic axis are both about 1.0m. It is expected that the significant beam attenuation and the beam slow down may be accompanied with the long paths.

A. Beam Attenuation

The probing beams will be attenuated with the interaction of the plasma, mainly with the electron ionization collisions. The beam attenuation rate is given by

$$\frac{\mathrm{d}I_{\mathrm{B}}(x)}{\mathrm{d}x} = -n_e(x)\left[\frac{S(T_e(x))}{v_{\mathrm{B}}}\right] I_{\mathrm{B}}(x) \tag{5}$$

$$S(T_e) = \int \sigma(v_e) v_e f(v_e) \mathrm{d}^3 v_e \tag{6}$$

where I_p, $S(T_e)$, $\sigma(v_e)$ and v_{B} are the primary beam intensity, the ionization rate, the cross section of electron impact ionizations and the beam velocity, respectively.

The experimental cross section of electron impact ionization is not available for gold and thallium. Here we use the cross section from the Lotz's empirical formula[15], which is represented as

$$\sigma = 4.5 \times 10^{-14} \sum_{i=1}^{N} \xi_i \frac{\ln(E/I_i)}{EI_i} \qquad [\mathrm{cm}^2] \tag{7}$$

$$S(T_e) = 3.0 \times 10^{-6} \sum_{i=1}^{N} \frac{\xi_i}{T_e[eV]^{1/2} I_i} \int_{I_i/T_e}^{\infty} \frac{\exp[-x]}{x} \mathrm{d}x \ , \qquad [\mathrm{cm}^3/\mathrm{s}] \tag{8}$$

where E_i, I_i and ξ_i are the beam energy, the ionization potential and the number of the equivalent electrons of the atom, respectively. However, this formula tends to give a smaller value than the actual one since this formula neglects the auto-ionization process which plays an important role in larger atoms. Figure 5 presents the ionization rates of gold calculated from the Lotz's formula as a function of the electron temperature. The atomic structure of neutral gold is $[Xe][4f^{14}5d^{10}]6s$. The following parameters are substituted into the formula; the numbers of the equivalent electrons and the corresponding ionization potentials of Au^+, Au^{2+} are 24, 23, $I_2(Au) = 20.5\mathrm{eV}$, $I_3(Au) = 30\mathrm{eV}$, respectively.

The solution of Eq. (5) can be written explicitly as

$$I_{\rm B} = I_{\rm B}(0) \exp\left[- \int n_{\rm e}(\xi) \left(\frac{S(T_e(\xi))}{v_{\rm b}} \right) {\rm d}\xi \right] . \tag{9}$$

Hence, the detectable secondary beam current can be expressed as

$$\begin{aligned} I_{\rm s} &= 2 I_{\rm p}(x_{\rm obs}) n_e(x_{\rm obs}) \left[\frac{S_{12}(T_e(x_{\rm obs}))}{v_{\rm B}} \right] \Delta l \exp\left[- \int_{x_{\rm obs}}^{x_{\rm out}} n_e(\xi) \left(\frac{S_{23}(T_e(\xi))}{v_{\rm B}} \right) {\rm d}\xi \right] \\ &= 2 I_{\rm p}(0) n_e(x_{\rm obs}) \left[\frac{S_{12}(T_e(x_{\rm obs}))}{v_{\rm B}} \right] \Delta l \\ &\times \exp\left[- \int_{x_{\rm in}}^{x_{\rm obs}} n_e(\xi) \left(\frac{S_{12}(T_e(\xi))}{v_{\rm B}} \right) {\rm d}\xi - \int_{x_{\rm obs}}^{x_{\rm out}} n_e(\xi) \left(\frac{S_{23}(T_e(\xi))}{v_{\rm B}} \right) {\rm d}\xi \right] , \end{aligned} \tag{10}$$

where $I_{\rm s}$, Δl, $x_{\rm obs}$, $x_{\rm in}$, $x_{\rm out}$, $S_{ij}(T_e)$ are the secondary beam current, the sample volume length, the ionization point, the entrance point of the primary beam into the plasma, the exit point of the secondary beam from the plasma, the ionization rate from i-th to j-th charged state, respectively. Figure 6 shows the expected secondary current for the 5.6MeV and 1.4MeV gold beams as a function of the central electron temperature, where the electron density and temperature profiles are assumed to be flat and parabolic, respectively, and the sample volume length is assumed to be 2cm. The secondary current is normalized by the injected primary beam current for several different electron densities.

The ionization cross-section used in this calculation includes only the process to the next charged state, although the other processes that more than two electrons are stripped simultaneously can not be neglected. In the energy range of our beam protons should also contribute to the impact ionization of the beam. Thus, the estimation gives an upper limit of the detectable secondary currents. In the 1.4MeV thallium beam for the operation of half magnetic field, it is expected that the ionization rates should be similar

to that of gold since the ionization potentials and the numbers of equivalent electrons are almost same; the atomic structures of neutral thallium is $[Xe][4f^{14}5d^{10}][6s^26p]$, and the ionization potentials are $I_2(T_l) = 20.428\text{eV}$, $I_3(T_l) = 29.83\text{eV}$.

The present calculation concludes that the current detection mode is not available even in the lower density plasma, particularly for the operation of half magnetic field, owing to the strong beam attenuation. A pulse counting method will be adopted for the beam detection in the LHD HIBP. Thus, the measurements of the density or potential fluctuations with high frequencies may be difficult.

C. Slowing-down of Probing Beam

Multi-times Coulomb collisions with ions and electrons in the plasma should result in significant reduction of the probing beam energy, as well as its intensity, due to the long path in the LHD plasma. The equation describing the beam energy attenuation is given by

$$\frac{\mathrm{d}E_\mathrm{B}}{\mathrm{d}x} = -\frac{2}{v_\mathrm{B}}\left(\frac{1}{\tau_\mathrm{se}(x)} + \frac{1}{\tau_\mathrm{si}(x)}\right)E_\mathrm{B} \tag{11}$$

where E_B, v_B, $\tau_\mathrm{se}(x)$ and $\tau_\mathrm{si}(x)$ are the beam energy, the beam velocity, the slowing down times due to the electrons and the ions, respectively. The product of the beam velocity and the slowing down time gives the attenuation length of energy as follows,

$$\begin{aligned} l_{s\alpha}(x) = 2v_\mathrm{B}\tau_{s\alpha}(x) &= 2\sqrt{\frac{2E_\mathrm{B}}{M_\mathrm{B}}} \times \frac{2^{3/2}\varepsilon_0^2 M_\mathrm{B}^{3/2} E_\mathrm{B}^{3/2}}{q_\mathrm{B}^2 q_\alpha^2 \left(1+\frac{M_\mathrm{B}}{m_\alpha}\right) n_\mathrm{e}(x)\mu(\zeta)\log\Lambda} \\ &= \frac{8\varepsilon_0^2 M_\mathrm{B} E_\mathrm{B}^2}{q_\mathrm{B}^2 q_\alpha^2 \left(1+\frac{M_\mathrm{B}}{m_\alpha}\right) n_\mathrm{e}(x)\mu(\zeta)\log\Lambda} \quad [\mathrm{m}] \end{aligned} \tag{12}$$

$$\zeta = \frac{m_\alpha v_B^2}{2T_\alpha}\,, \quad \mu(\zeta) = \frac{2}{\sqrt{\pi}} \int_0^\zeta \sqrt{\xi} \exp[-\xi] d\xi \tag{13}$$

where α represent the field particles (proton, electron). The slowing down time can be estimated from the formula derived by Chandrasekhar. Figure 7 shows the attenuation lengths as a function of beam energy for three different proton and electron temperatures under the assumption that the electron density and the charge of beam are $1 \times 10^{20}/\mathrm{m}^3$, $q_\alpha = q_B = 1$, respectively. The proton contribution to the beam energy reduction is much stronger in lower beam energy, while the electrons give almost same contributions in MeV range.

Assuming that the beam energy in the expression of the slowing down time τ should be constant, the solution of Eq. (11) is easily obtained as

$$E_B = E_B(0) \exp\left[- \int \frac{2}{v_B} \left(\frac{1}{\tau_{se}(\xi)} + \frac{1}{\tau_{si}(\xi)} \right) d\xi \right] . \tag{14}$$

The beam energy reduction for the probing beam trajectory to observe the magnetic axis is easily calculated using this formula. The results are shown as a function of the central temperature in Fig. 8 for several different electron density cases; the electron density and temperature profiles are assumed to be flat and parabolic, respectively, and the ion temperature is assumed to be equal to that of electron. When $T_e = 2\mathrm{keV}$, the energy reduction of 5.6MeV beam is about 100eV for $1 \times 10^{20}\mathrm{m}^{-3}$. Consequently, in the higher density plasma it should be careful to measure the absolute potential.

IV. Energy Analyzer Candidates

A. Operation Voltage of Cylindrical Analyzer

30° parallel plate energy analyzers have been traditionally used for the energy analyzers of HIBP owing to its second order focusing property which

diminish the measurement error caused by the difference of beam injection angle into the analyzer[17-22]. However, its operation voltage for analyzing 6MeV beams ($\simeq$1MeV) is far beyond the practical limit. Thus, a new kind of energy analyzer is indispensable to realize the 6MeV HIBP.

The most feasible candidate is, so far, cylindrical type energy analyzers; this analyzer uses the electric field efficiently, so that the applied voltage on the electrodes can be small[23-25]. The operation voltage is related to the gap width between the electrodes as follows;

$$V_{\rm op} \simeq \frac{2K_0}{q}\frac{d}{R_0}\,, \tag{15}$$

where q, d, R_0 represent the charge of beam particle, the half width of the gap, the radius of the standard beam trajectory ($r = R_0$), respectively. The half width d can not be reduced to the maximum radial displacement from the central trajectory. Since the maximum displacement increases with the beam incident angle, our requirements of small operation voltage is, in principle, not compatible with the wide acceptance of the beam incident angle. When the operation voltage is 60keV for 6MeV secondary beam, the ratio of the half width to the major radius is $d/R_0 \simeq 1/100$. Then, the gap width $2d$ of 5cm yields R_0 =2.5m. The dimension of the analyzer is large but practical as shown in Fig. 1.

B. Focus Properties of Cylindrical Analyzer

As it is well known, the 127.3° energy analyzer has a first focusing property, which may be insufficient for the HIBP application where the beam energy should be measured with a precision of $10^{-4} \sim 10^{-5}$. Consequently, the acceptance angle widow is required to be as wide as possible. There exits a possibility that the focus property may be improved in the cylindrical an-

alyzers if drift spaces are equipped in front of both entrance and exit of the cylinder. A theoretical study[25] was executed to confirm this proposition. In the analysis, the treatment of the fringing field penetrating into the drift regions around the ends of cylinder is essential since the fringing field should affect even the focus property of first order; the effects are mainly divided into alternation of the beam velocity and deflection of beam at the cylinder ends.

One of the main results of the analysis is that the second order focus can be achieved when the angle length is larger than 127.3°. Therefore, the acceptance angle become remarkably wider than that of 127.3° if the angle length is properly chosen. However, the energy resolution of this type is predicted to be worse than the traditional 127.3°. The focus property is evaluated in a Taylor expansion of the beam displacement Δr with respect to the beam incident angle $\Delta\theta$;

$$\Delta r(\Delta\theta,\ \Delta K_0) = c_0(\phi_0) + c_1(\phi_0)\Delta\theta + c_2(\phi_0)\Delta\theta^2 + \cdots + \left(\frac{\partial r}{\partial K_0}\right)\Delta K_0\ , \quad (16)$$

where $\partial r/\partial K_0$ means the energy resolution. If the first and second order coefficients are zero ($c_1(\phi_0) = c_2(\phi_0) = 0$), second order focusing is realized.

Figure 9 shows the relations between the drift region lengths of the entrance and exit sides h and l to be consistent with the first order focusing for 105° , 210° cylindrical analyzers. Note that the dimension of lengths is normalized by R_0, the fringing field is assumed to be confined within the region whose distance from the cylinder end is $\delta = 0.1$. Figure 10 indicates the second order coefficients $c_2(\phi_0)$ and the energy resolutions of 105°, 210° as a function of the entrance drift region length h. In the case of 210° analyzer, the second order focusing is achieved when the drift region lengths $h = 0.160$, $l = 0.552$, and the second order coefficient has a small value over

wide range of $0.1 \leq h \leq 0.5$. On the other hand, the 105° analyzer has much better energy resolution although there is no focal length to make the second order coefficient zero.

IV. Summary

The heavy ion beam probe application on the LHD may be one of the most challenging projects, and there exist several problems to be overcome as follows.

i) In order to manage the 3-D probing trajectories in a helical magnetic field, we will introduce two sets of sweep plates in front of the energy analyzer. For avoiding the voltage break-down due to the strong UV radiation from the LHD plasma, some new ideas for the voltage reduction should be incorporated into the design of the sweep plates.

ii) A new method of the secondary beam detection, a particle counting method, should be essential since the beam attenuation caused by the long paths ($\simeq$ 2m) of the probing beam trajectories in the plasma is too severe for the secondary beam to be detected as beam current. The energy reduction due to the multiple Coulomb collisions with ions and electrons in the plasma should be taken into account for precise measurements of absolute plasma potential.

iii) A cylindrical analyzer owing the second order focusing is the most feasible candidate for MeV range heavy ion beam probe as a substitution of the traditional 30° parallel plate energy analyzer. A prototype should be constructed, and the properties of focus and energy resolution power should be examined. The tolerance of the acceptance angle window of

analyzer is deeply related to the achievement of the active trajectory control.

The intense researches and developments should be necessary to realize the potential measurements with the heavy ion beam probe method for the LHD plasma.

References

[1] F. C. Jobes and R. L. Hickok, "A Direct Measurements of Plasma Space Potential", Nucl. Fusion, **10**, 195-197(1970).

[2] J. C. Hosea, F. C. Jobes, R. L. Hickok and A. N. Dillis, "Rotation and Structure of Low Frequency Oscillations inside the ST-Tokamak Plasma", Phys. Rev. Lett. **30**, 839-842(1973).

[3] F. M. Bieniosek, P. L. Colestock, K. A. Connor, R. L. Hickok, S. P. Kuo, R. A. Dandl, "Elmo Bumpy Torus Heavy Ion Beam Probe", Rev. Sci. Instrum. **51**, 206-212(1980).

[4] P. M. Schoch, J. C. Forster, W. C. Jennings and R. L. Hickok, "TEXT Heavy Ion Beam Probe System", Rev. Sci. Intrum. **57**, 1825-1827(1986).

[5] R. L. Hickok and P. M. Schoch, "Proposed 2MeV Beam Probe System for TEXT-upgrade", Rev. Sci. Intrum. **59**, 1685-1987(1988).

[6] T. P. Crowley, P. M. Schoch, J. W. Heard, R. L. Hickok, X. Yang, "Heavy Ion Beam Probe Wavenumber Measurements from the Text Tokamak Edge", Nucl. Fusion **32**, 1295-1311(1992).

[7] G. A. Hallock, J. Mathew, W. C. Jennings, and R. L. Hickok, "Space Potential Distribution in the ISX-B Tokamak", Phys. Rev. Lett. **56**, 1248-1251(1986).

[8] K. Takasugi, H. Iguchi, M. Fujiwara, H. Ikegami, " Heavy Ion Beam Probe for the Study of Plasma Confinement in Nagoya Bumpy Torus", Jpn. J. Appl. Phys. **23**, 364-372(1984).

[9] H. Iguchi, K. Takasugi, T. Shoji, J. Fujita, H. Ikegami, "Simultaneous Measurements of Plsama Potential and Density Fluctuations in Bumpy Torus by Heavy Ion Beam Probe", Jpn. J. Appl. Phys. **32**, 1829-1834(1993).

[10] J. J. Zielinski, S. C. Aceto, K. A. Connor et al., "ATF Heavy Ion Beam Probe: Installation and Initial Operation", Rev. Sci. Instrum. **61**, 2961-2963(1990).

[11] A. Carnevali, K. A. Connor, S. C. Aceto, et al., "Heavy Ion Beam Probe for the Advanced Toroidal Facility", Rev. Sci. Instrum. **59**, 1670-1672(1988).

[12] A. Carnevali, J. R. Misium, J. F. Lewis, and K. A. Connor, "Heavy Ion Beam Probe Diagnostic System for Stellarators", Rev. Sci. Instrum. **57**, 1822-1824(1986).

[13] A. Fujisawa, H. Iguchi, M. Sasao, Y. Hamada and J. Fujita, "Active Control of Beam Trajectories for Heavy Ion Beam Probe on Helical Magnetic Configurations", Rev. Sci. Instrum. **63**, 3694-3700(1992)

[14] M. Sasao, Y. Okabe, A. Fujisawa, J. Fujita, H. Yamaoka, M. Wada,

"Development of Negative Heavy Ion Beam Sources for Plasma Potential Measurements", Rev. Sci. Instrum. **63**, 2726-2728(1992).

[15] W. Lotz, "Electron-Impact Ionization Cross-Sections and Ionization Rate Coefficients for Atoms and Ions", Astrophy. J. Suppl. **14**, 207-238(1967).

[16] S. I. Braginskii, "Transport Processes in a Plasma", Rev. of Plasma Phys. Vol. 4, 205-311 (ed by M. A. Leontovich), Consultants Bureau, New York 1966.

[17] T. S. Green and G. A. Proca, "A Parallel Plate Electrosttic Spectrograph", Rev. Sci. Instrum. **41**, 1409-1414(1970).

[18] G. A. Proca and T. S. Green, "Minimum Image Size in a Parallel Plate Electrostatic Spectrograph", Rev. Sci. Instrum. **41**, 1778-1783(1970).

[19] L. Solensten and K. A. Connor, "Heavy Ion Beam Probe Energy Analyzer for Measurements of Plasma Potential Fluctuation", Rev. Sci.Instrum. **58**, 516-519(1987).

[20] S. C. Aceto, K. A. Connor, P. E. McClaren, J. J. Zielinski, and J. G. Schatz, "Energy Analyzer for the ATF Heavy Ion Beam Probe", Rev. Sci. Instrum. **61**, 2958-2960(1990).

[21] P. E. McClaren, K. A. Connor, J. F. Lewis, R. L. Hickok, T. P. Crowley, J. G. Schatz and G. H. Vilardi, "Electric Field Studies of 2MeV Electrostatic Energy Analyzer", Rev. Sci. Instrum. **61**, 2955-2957(1990).

[22] Y. Hamada, Y. Kawasumi, K. Masai, H. Iguchi, A. Fujisawa, Y. Abe, "Shaped Electrode System for High Voltage Parallel Plate Analyzer", Rev. Sci. Instrum. **63**, 4446-4449(1992).

[23] K. A. Connor, T. P. Crowley, R. L. Hickok, A. Carnevali, P. M. Schoch, J. Resnick V. Simicic, J. G. Schatz, J. Heard, S. C. Aceto, and J. F. Lewis, "Advances in Heavy Ion Beam Probing", Rev. Sci. Instrum. **59**, 1673-1675(1988).

[24] H. J. Leisenfelder. R. L. Hickok, J. H. Resnick, T. P. Crowley and J. G. Schatz, "Electrostatic Energy Analyzer for Multi-MeV Heavy Ion Beam Probes", Rev. Sci. Instrum. **63**, 4579-4581(1992).

[25] A. Fujisawa, Y. Hamada, "Theoretical Study of Cylindrical Energy Analyzer for MeV Range Heavy Ion Beam Probes", Rev. Sci. Instrum. **64**, 3503-3514(1993).

Figure Captions

Fig. 1: A schematic view of the 6MeV heavy ion beam probe on the Large Helical Device.

Fig. 2: (a) Electric fields of four sets of sweep plates as a function of the toroidal angle of the observation point $\xi_{\rm ion}$ (b) corresponding observation points.

Fig. 3: Examples of probing beam trajectories; (a)top view (b) side view. The secondary beam trajectories pass at a fixed point (shown by a circle) with a constant angle. The other circles mean the cross points between trajectories and the side and bottom ports planes. The x-points indicate the ionization positions. The rectangles represent the regions where electric fields of sweep plates exist.

Fig. 4: Probing beam path lengths in the LHD plasma as a function of the toroidal angle of the observation point $\xi_{\rm ion}$.

Fig. 5: Electron impact ionization cross section of gold expected from Lotz's empirical formula.

Fig. 6: Dependence of gold beam attenuation on the central electron temperature. The electron temperature and density profiles are assumed to be parabolic and flat, respectively. (a)5.6MeV beam for the 3T standard operation (b)1.4MeV beam for the half magnetic field operation.

Fig. 7: Slowing down times as a function of electron or proton temperature.

Fig. 8: Dependence of beam energy attenuation on the central plasma temperature. The electron and proton have the same temperature and

the temperature and density profiles are assumed to be parabolic and flat, respectively. (a)5.6MeV beam for the 3T standard operation (b)1.4MeV beam for the half magnetic field operation.

Fig. 9: Relations between the drift regions h, l lengths when the first order focus is achieved for two cylindrical energy analyzers; (a)$\phi_0 = 210°$ (b)$\phi_0 = 105°$.

Fig. 10: Focus properties and energy resolutions of cylindrical analyzers; (a)$\phi_0 = 210°$ (b)$\phi_0 = 105°$.

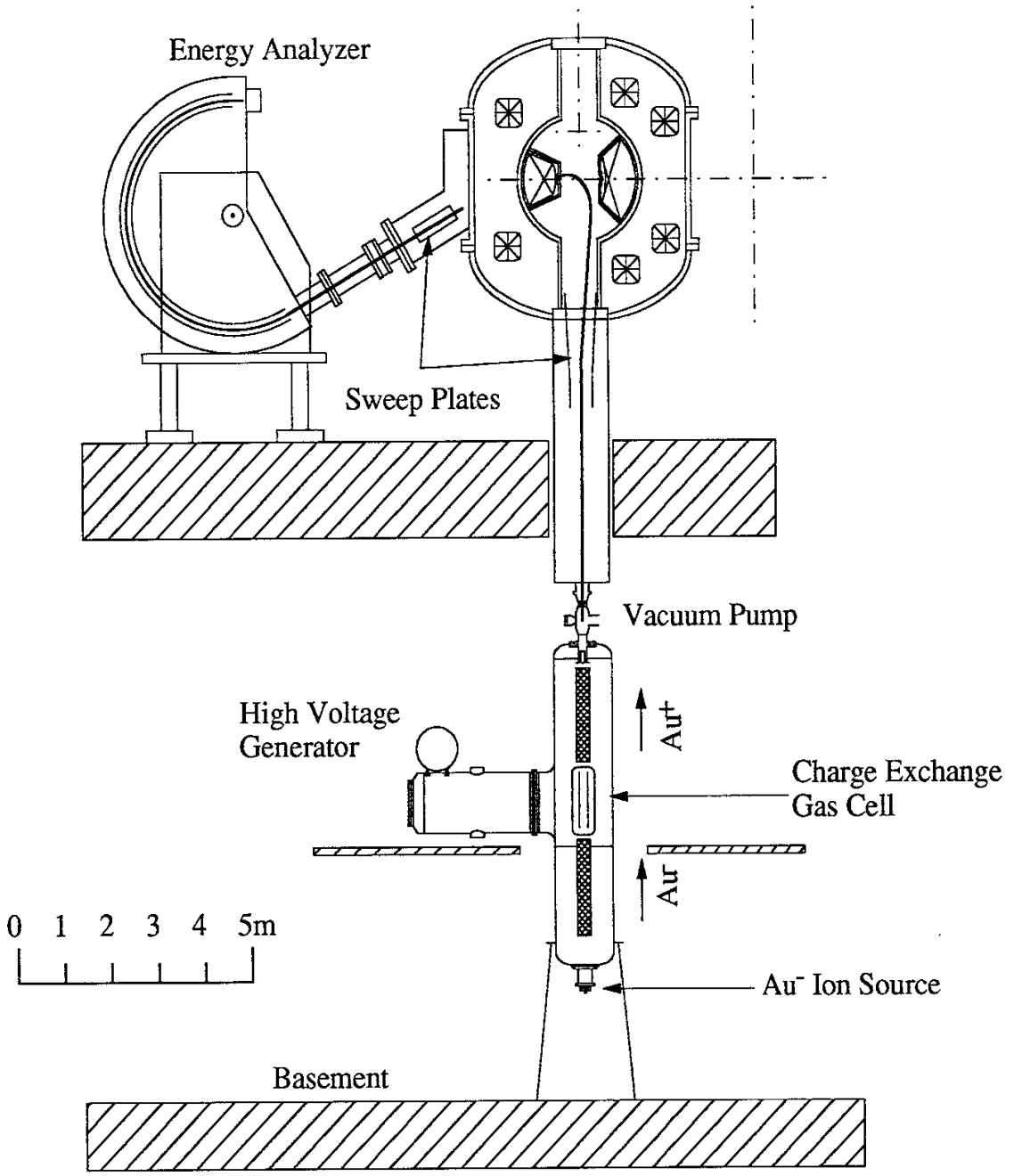

Fig. 1 A. Fujisawa, H. Iguchi, A. Taniike, M. Sasao, Y. Hamada

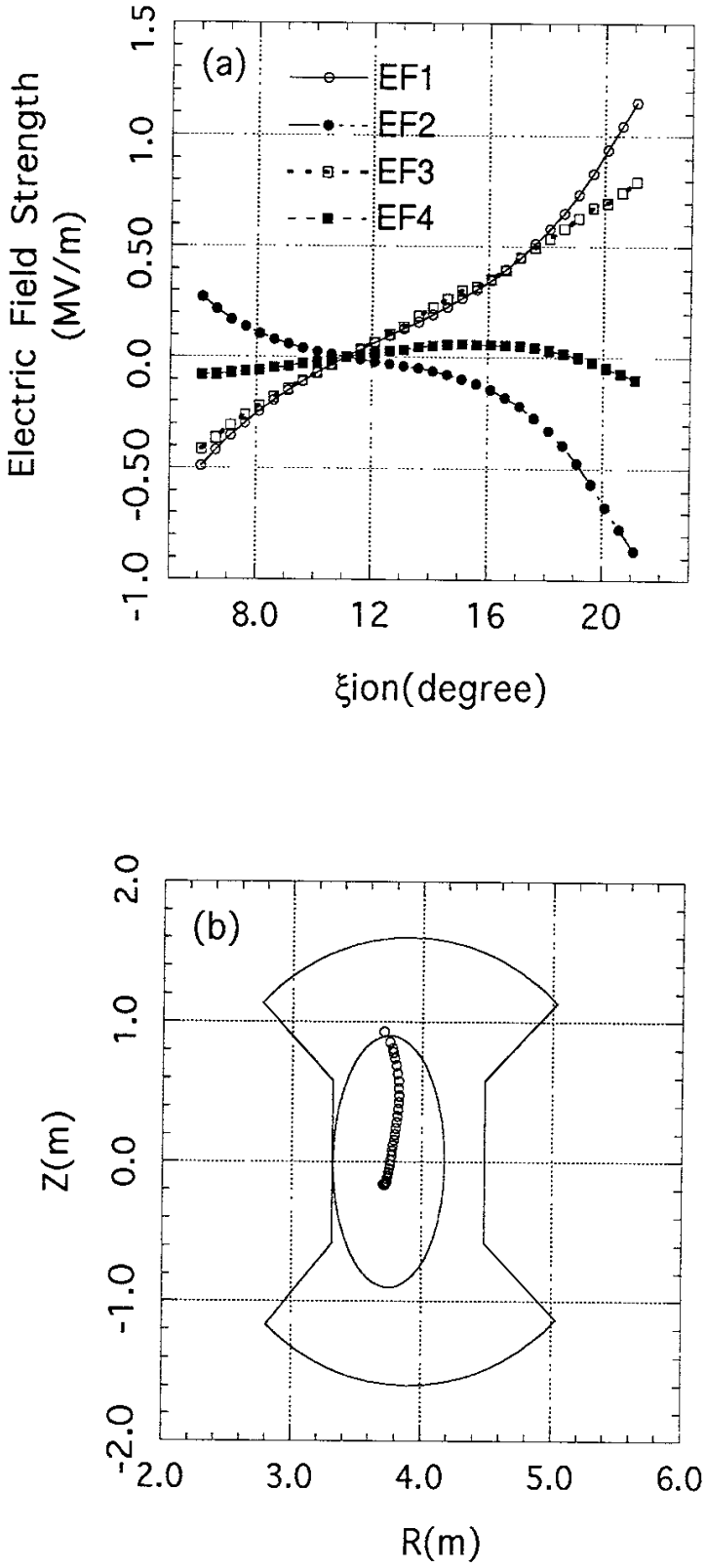

Fig. 2 A. Fujisawa, H. Iguchi, A. Taniike, M. Sasao, Y. Hamada

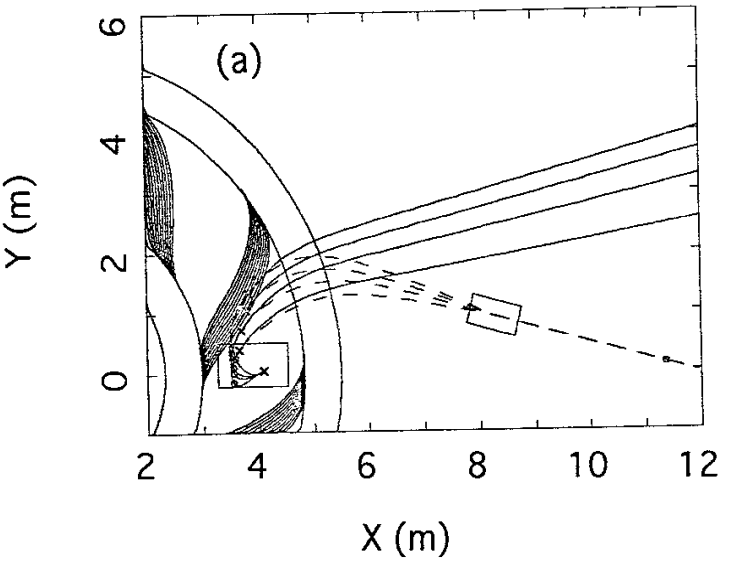

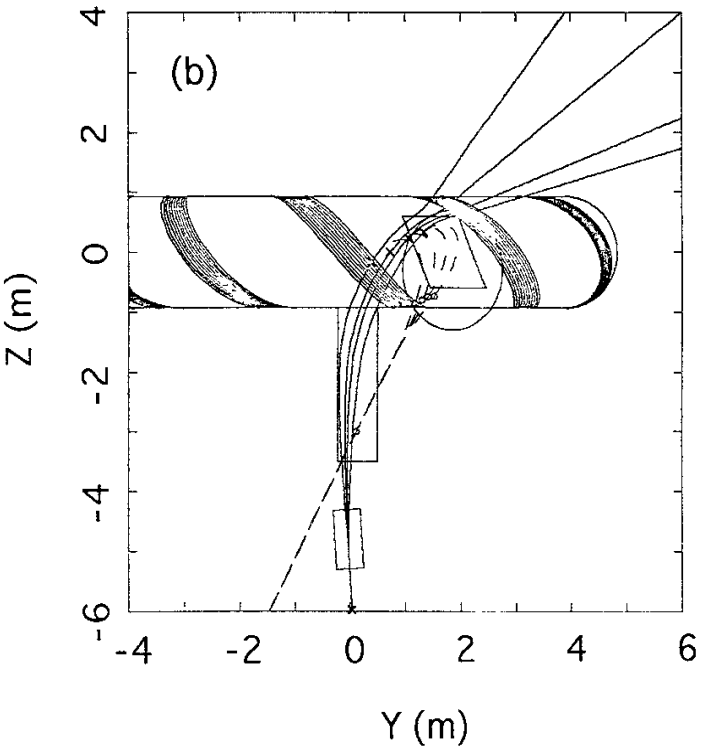

Fig. 3 A. Fujisawa, H. Iguchi, A. Taniike, M. Sasao, Y. Hamada

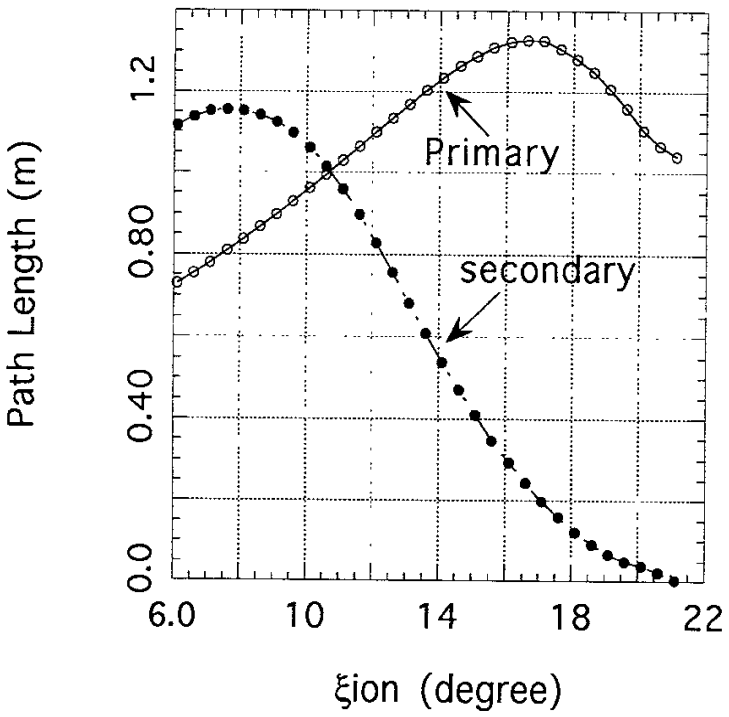

Fig. 4 A. Fujisawa, H. Iguchi, A. Taniike, M. Sasao, Y. Hamada

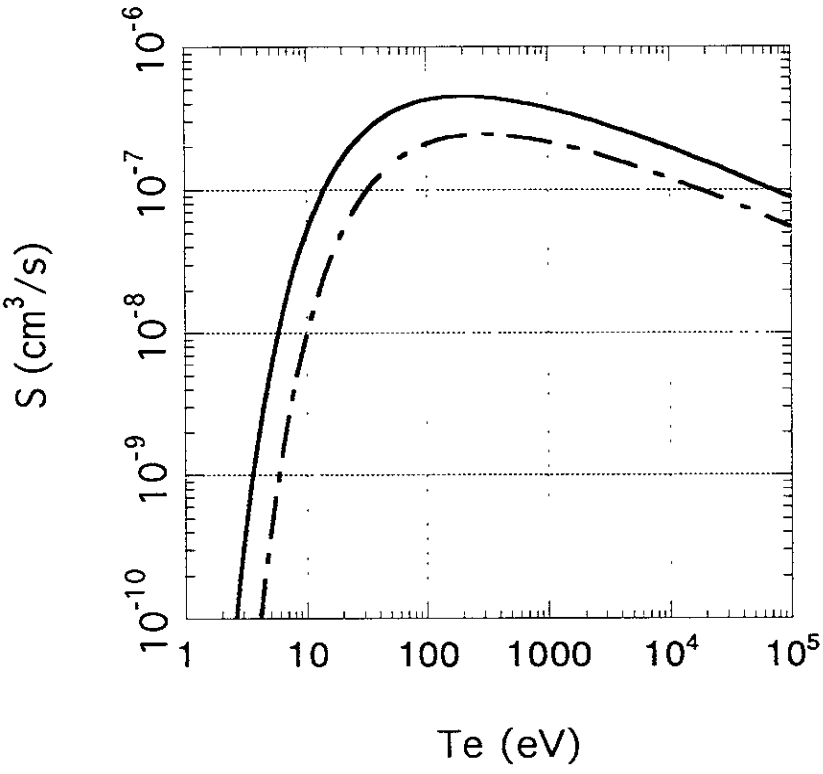

Fig. 5 A. Fujisawa, H. Iguchi, A. Taniike, M. Sasao, Y. Hamada

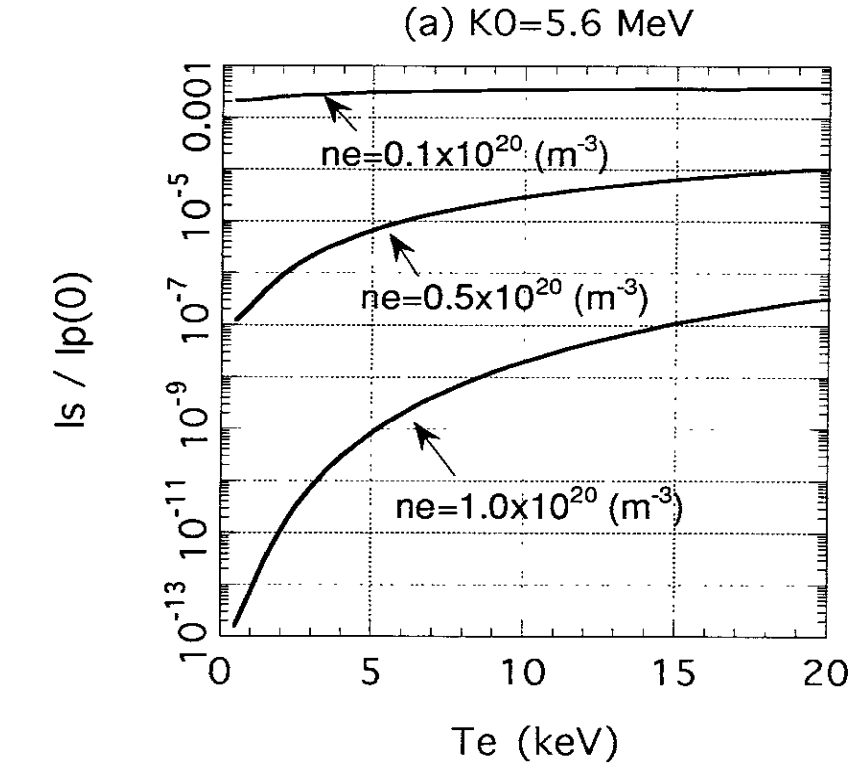

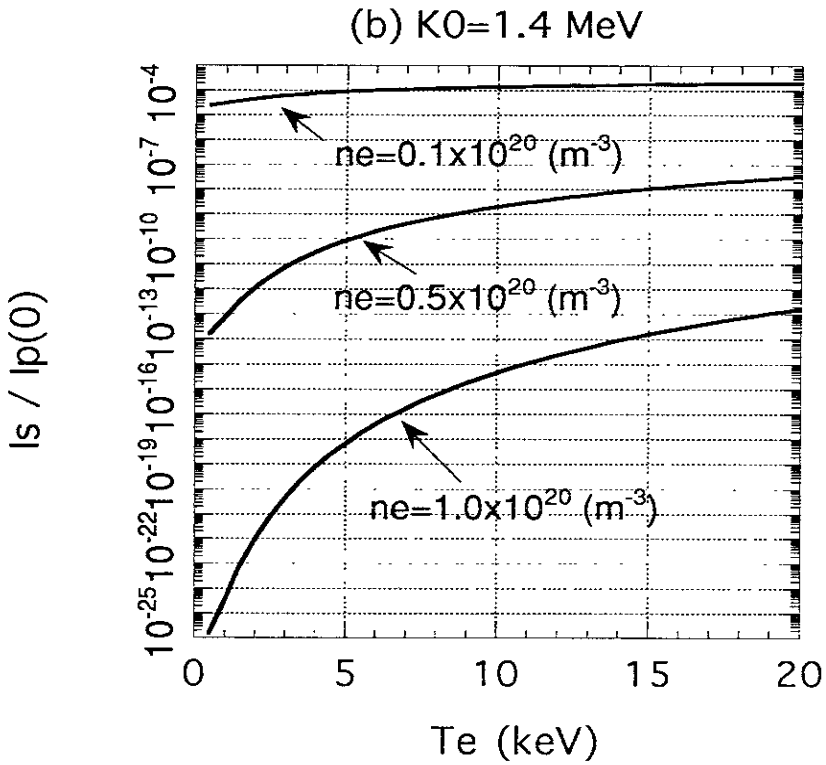

Fig. 6 A. Fujisawa, H. Iguchi, A. Taniike, M. Sasao, Y. Hamada

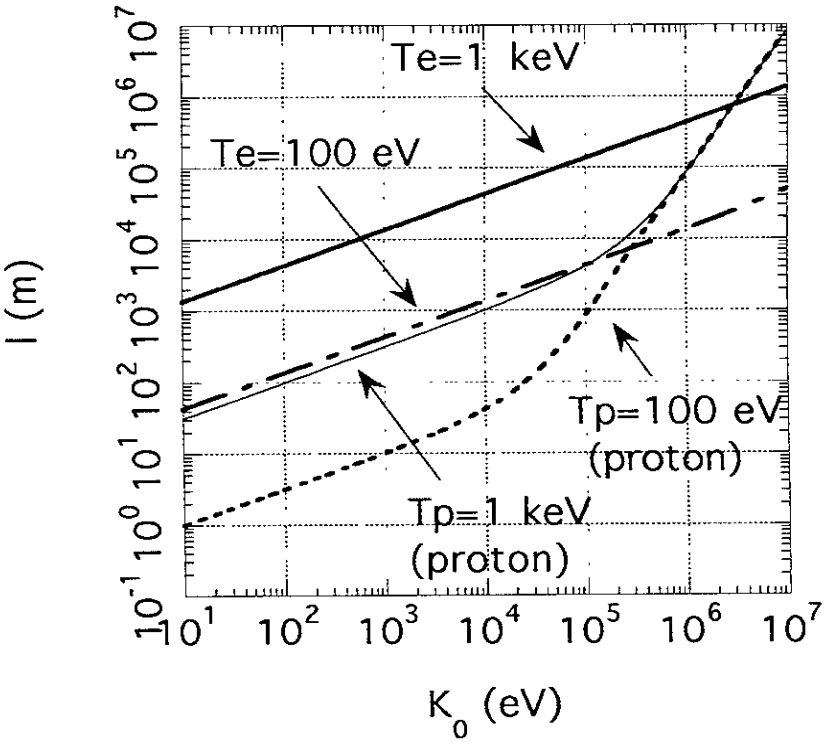

Fig. 7 A. Fujisawa, H. Iguchi, A. Taniike, M. Sasao, Y. Hamada

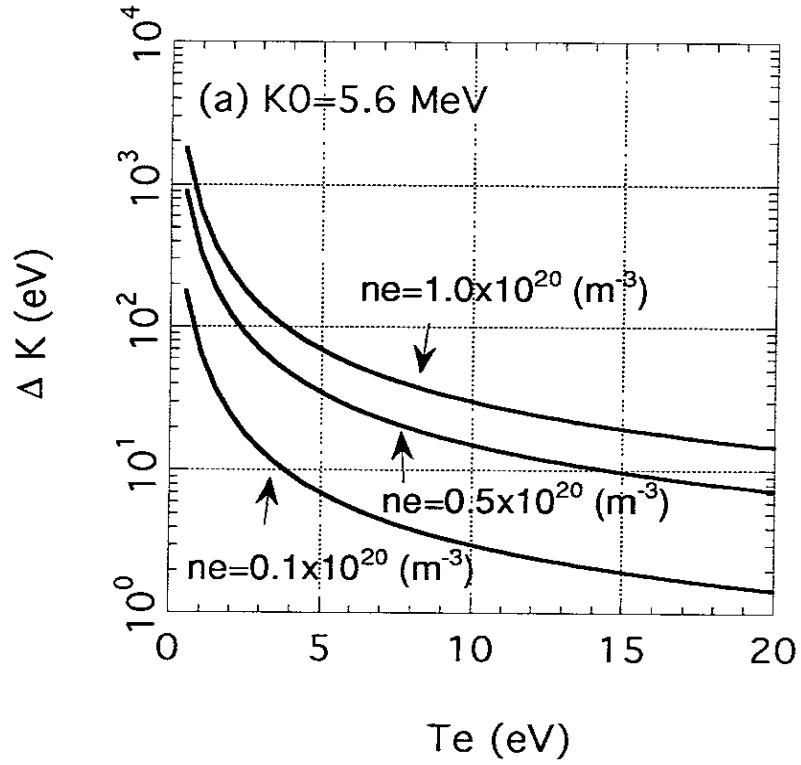

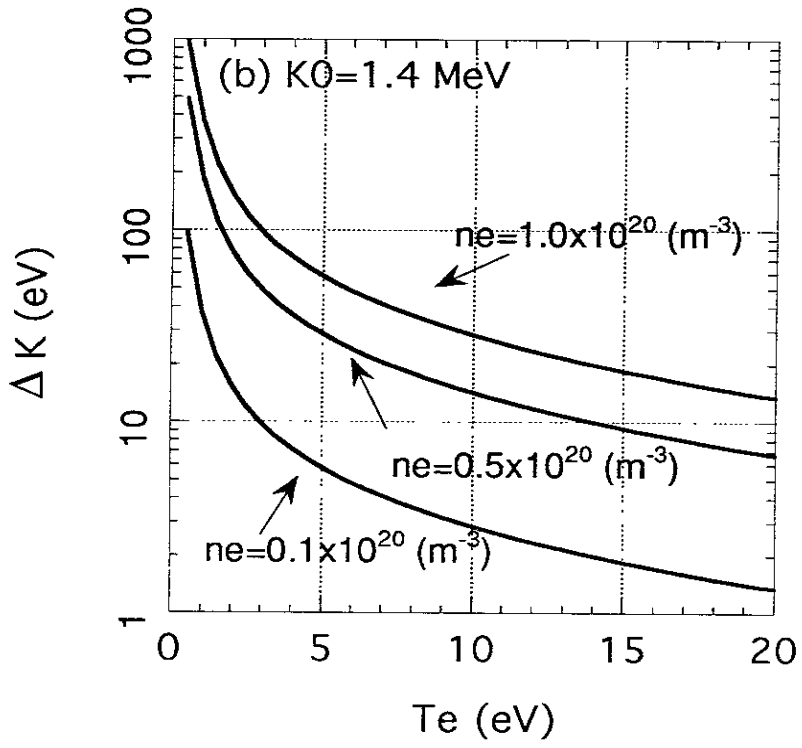

Fig. 8 A. Fujisawa, H. Iguchi, A. Taniike, M. Sasao, Y. Hamada

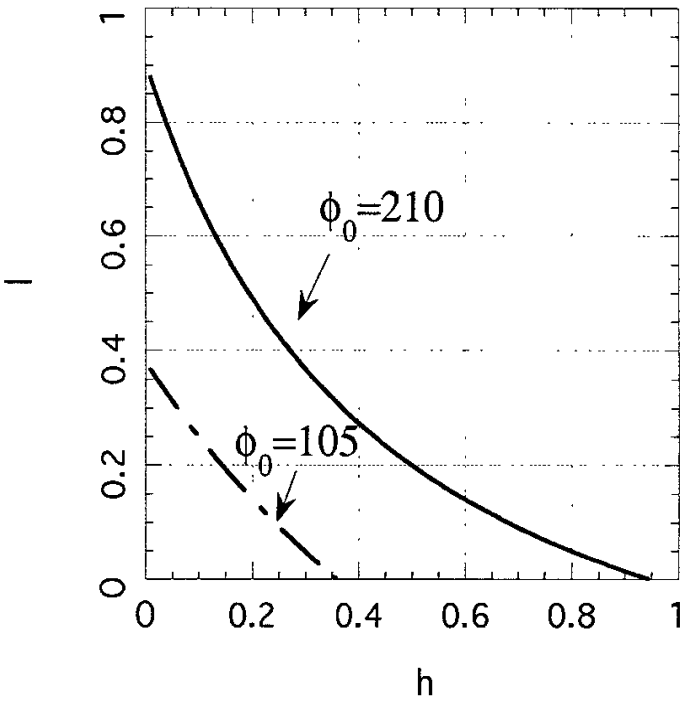

Fig. 9 A. Fujisawa, H. Iguchi, A. Taniike, M. Sasao, Y. Hamada

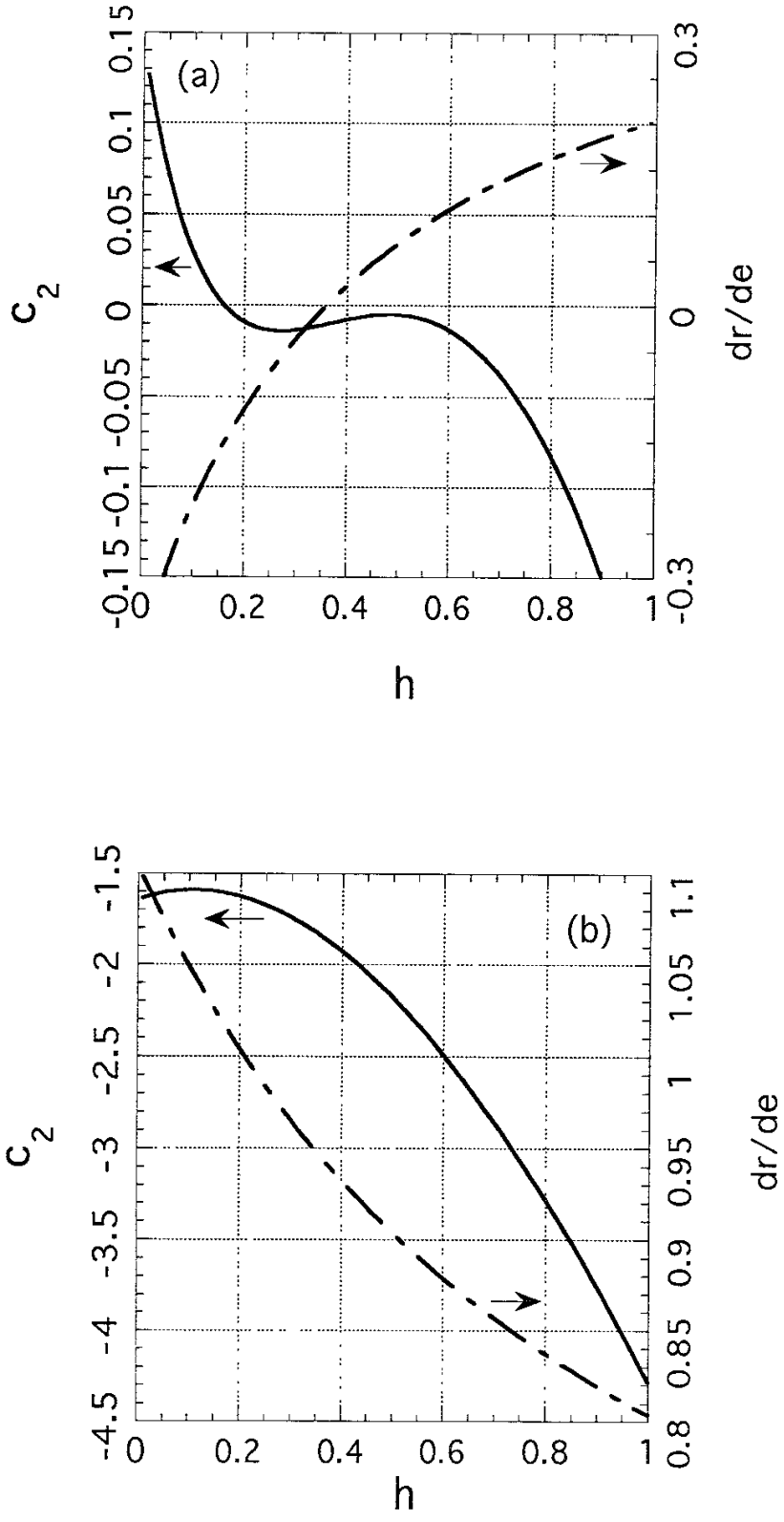

Fig. 10 A. Fujisawa, H. Iguchi, A. Taniike, M. Sasao, Y. Hamada

Recent Issues of NIFS Series

NIFS-223 K. Itoh, S.-I. Itoh, M. Yagi, A. Fukuyama and M. Azumi, *Theory of Pseudo-Classical Confinement and Transmutation to L-Mode;* May 1993

NIFS-224 M. Tanaka, *HIDENEK: An Implicit Particle Simulation of Kinetic-MHD Phenomena in Three-Dimensional Plasmas;* May 1993

NIFS-225 H. Hojo and T. Hatori, *Bounce Resonance Heating and Transport in a Magnetic Mirror;* May 1993

NIFS-226 S.-I. Iton, K. Itoh, A. Fukuyama, M. Yagi, *Theory of Anomalous Transport in H-Mode Plasmas;* May 1993

NIFS-227 T. Yamagishi, *Anomalous Cross Field Flux in CHS ;* May 1993

NIFS-228 Y. Ohkouchi, S. Sasaki, S. Takamura, T. Kato, *Effective Emission and Ionization Rate Coefficients of Atomic Carbons in Plasmas;* June 1993

NIFS-229 K. Itoh, M. Yagi, A. Fukuyama, S.-I. Itoh and M. Azumi, *Comment on 'A Mean Field Ohm's Law for Collisionless Plasmas;* June 1993

NIFS-230 H. Idei, K. Ida, H. Sanuki, H. Yamada, H. Iguchi, S. Kubo, R. Akiyama, H. Arimoto, M. Fujiwara, M. Hosokawa, K. Matsuoka, S. Morita, K. Nishimura, K. Ohkubo, S. Okamura, S. Sakakibara, C. Takahashi, Y. Takita, K. Tsumori and I. Yamada, *Transition of Radial Electric Field by Electron Cyclotron Heating in Stellarator Plasmas;* June 1993

NIFS-231 H.J. Gardner and K. Ichiguchi, *Free-Boundary Equilibrium Studies for the Large Helical Device,* June 1993

NIFS-232 K. Itoh, S.-I. Itoh, A. Fukuyama, H. Sanuki and M. Yagi, *Confinement Improvement in H-Mode-Like Plasmas in Helical Systems,* June 1993

NIFS-233 R. Horiuchi and T. Sato, *Collisionless Driven Magnetic Reconnection,* June 1993

NIFS-234 K. Itoh, S.-I. Itoh, A. Fukuyama, M. Yagi and M. *Azumi, Prandtl Number of Toroidal Plasmas;* June 1993

NIFS-235 S. Kawata, S. Kato and S. Kiyokawa , *Screening Constants for Plasma;* June 1993

NIFS-236 A. Fujisawa and Y. Hamada, *Theoretical Study of Cylindrical Energy*

Analyzers for MeV Range Heavy Ion Beam Probes; July 1993

NIFS-237 N. Ohyabu, A. Sagara, T. Ono, T. Kawamura and O. Motojima, *Carbon Sheet Pumping;* July 1993

NIFS-238 K. Watanabe, T. Sato and Y. Nakayama, *Q-profile Flattening due to Nonlinear Development of Resistive Kink Mode and Ensuing Fast Crash in Sawtooth Oscillations;* July 1993

NIFS-239 N. Ohyabu, T. Watanabe, Hantao Ji, H. Akao, T. Ono, T. Kawamura, K. Yamazaki, K. Akaishi, N. Inoue, A. Komori, Y. Kubota, N. Noda, A. Sagara, H. Suzuki, O. Motojima, M. Fujiwara, A. Iiyoshi, *LHD Helical Divertor;* July 1993

NIFS-240 Y. Miura, F. Okano, N. Suzuki, M. Mori, K. Hoshino, H. Maeda, T. Takizuka, JFT-2M Group, K. Itoh and S.-I. Itoh, *Ion Heat Pulse after Sawtooth Crash in the JFT-2M Tokamak;* Aug. 1993

NIFS-241 K. Ida, Y.Miura, T. Matsuda, K. Itoh and JFT-2M Group, *Observation of non Diffusive Term of Toroidal Momentum Transport in the JFT-2M Tokamak;* Aug. 1993

NIFS-242 O.J.W.F. Kardaun, S.-I. Itoh, K. Itoh and J.W.P.F. Kardaun, *Discriminant Analysis to Predict the Occurrence of ELMS in H-Mode Discharges;* Aug. 1993

NIFS-243 K. Itoh, S.-I. Itoh, A. Fukuyama, *Modelling of Transport Phenomena;* Sep. 1993

NIFS-244 J. Todoroki, *Averaged Resistive MHD Equations;* Sep. 1993

NIFS-245 M. Tanaka, *The Origin of Collisionless Dissipation in Magnetic Reconnection;* Sep. 1993

NIFS-246 M. Yagi, K. Itoh, S.-I. Itoh, A. Fukuyama and M. Azumi, *Current Diffusive Ballooning Mode in Seecond Stability Region of Tokamaks;* Sep. 1993

NIFS-247 T. Yamagishi, *Trapped Electron Instabilities due to Electron Temperature Gradient and Anomalous Transport;* Oct. 1993

NIFS-248 Y. Kondoh, *Attractors of Dissipative Structure in Three Disspative Fluids;* Oct. 1993

NIFS-249 S. Murakami, M. Okamoto, N. Nakajima, M. Ohnishi, H. Okada,

Monte Carlo Simulation Study of the ICRF Minority Heating in the Large Helical Device; Oct. 1993

NIFS-250 A. Iiyoshi, H. Momota, O. Motojima, M. Okamoto, S. Sudo, Y. Tomita, S. Yamaguchi, M. Ohnishi, M. Onozuka, C. Uenosono,
Innovative Energy Production in Fusion Reactors; Oct. 1993

NIFS-251 H. Momota, O. Motojima, M. Okamoto, S. Sudo, Y. Tomita, S. Yamaguchi, A. Iiyoshi, M. Onozuka, M. Ohnishi, C. Uenosono,
Characteristics of D-^{3}He Fueled FRC Reactor: ARTEMIS-L,
Nov. 1993

NIFS-252 Y. Tomita, L.Y. Shu, H. Momota,
Direct Energy Conversion System for D-^{3}He Fusion, Nov. 1993

NIFS-253 S. Sudo, Y. Tomita, S. Yamaguchi, A. Iiyoshi, H. Momota, O. Motojima, M. Okamoto, M. Ohnishi, M. Onozuka, C. Uenosono,
Hydrogen Production in Fusion Reactors, Nov. 1993

NIFS-254 S. Yamaguchi, A. Iiyoshi, O. Motojima, M. Okamoto, S. Sudo, M. Ohnishi, M. Onozuka, C. Uenosono,
Direct Energy Conversion of Radiation Energy in Fusion Reactor,
Nov. 1993

NIFS-255 S. Sudo, M. Kanno, H. Kaneko, S. Saka, T. Shirai, T. Baba,
Proposed High Speed Pellet Injection System "HIPEL" for Large Helical Device
Nov. 1993

NIFS-256 S. Yamada, H. Chikaraishi, S. Tanahashi, T. Mito, K. Takahata, N. Yanagi, M. Sakamoto, A. Nishimura, O. Motojima, J. Yamamoto, Y. Yonenaga, R. Watanabe,
Improvement of a High Current DC Power Supply System for Testing the Large Scaled Superconducting Cables and Magnets; Nov. 1993

NIFS-257 S. Sasaki, Y. Uesugi, S. Takamura, H. Sanuki, K. Kadota,
Temporal Behavior of the Electron Density Profile During Limiter Biasing in the HYBTOK-II Tokamak; Nov. 1993

NIFS-258 K. Yamazaki, H. Kaneko, S. Yamaguchi, K.Y. Watanabe, Y.Taniguchi, O.Motojima, LHD Group,
Design of Central Control System for Large Helical Device (LHD);
Nov. 1993

NIFS-259 K. Yamazaki, H. Kaneko, S. Yamaguchi, K.Y. Watanabe, Y.Taniguchi, O.Motojima, LHD Group,
Design of Central Control System for Large Helical Device (LHD);
Nov. 1993

NIFS-260 B.V.Kuteev,
Pellet Ablation in Large Helical Device; Nov. 1993

NIFS-261 K. Yamazaki,
Proposal of "MODULAR HELIOTRON': Advanced Modular Helical System Compatible with Closed Helical Divertor; Nov. 1993

NIFS-262 V.D.Pustovitov,
Some Theoretical Problems of Magnetic Diagnostics in Tokamaks and Stellarators; Dec. 1993

NIFS-263 A. Fujisawa, H. Iguchi, Y. Hamada
A Study of Non-Ideal Focus Properties of 30° Parallel Plate Energy Analyzers; Dec. 1993

NIFS-264 K. Masai,
Nonequilibria in Thermal Emission from Supernova Remnants; Dec. 1993

NIFS-265 K. Masai, K. Nomoto,
X-Ray Enhancement of SN 1987A Due to Interaction with its Ring-like Nebula; Dec. 1993

NIFS-266 J. Uramoto
A Research of Possibility for Negative Muon Production by a Low Energy Electron Beam Accompanying Ion Beam; Dec. 1993

NIFS-267 H. Iguchi, K. Ida, H. Yamada, K. Itoh, S.-I. Itoh, K. Matsuoka, S. Okamura, H. Sanuki, I. Yamada, H. Takenaga, K. Uchino, K. Muraoka,
The Effect of Magnetic Field Configuration on Particle Pinch Velocity in Compact Helical System (CHS); Jan. 1993

NIFS-268 T. Shikama, C. Namba, M. Kosuda, Y. Maeda,
Development of High Time-Resolution Laser Flash Equipment for Thermal Diffusivity Measurements Usting Miniature-Size Specimens; Jan. 1994

NIFS-269 T. Hayashi, T. Sato, P. Merkel, J. Nührenberg, U. Schwenn,
Formation and 'Self-Healing' of Magnetic Islands in Finite-β Helias Equilibria; Jan. 1994

NIFS-270 S. Murakami, M. Okamoto, N. Nakajima, T. Mutoh,
Efficiencies of the ICRF Minority Heating in the CHS and LHD Plasmas; Jan. 1994

NIFS-271 Y. Nejoh, H. Sanuki,
Large Amplitude Langmuir and Ion-Acoustic Waves in a Relativistic Two-Fluid Plasma; Feb. 1994